ACS Photonics

Article

pubs.acs.org/journal/apchd5

Indium for Deep-Ultraviolet Surface-Enhanced Resonance Raman Scattering

Yasuaki Kumamoto,[†] Atsushi Taguchi,[†,‡] Mitsuhiro Honda,[‡] Koichi Watanabe,[‡] Yuika Saito,*[,‡] and Satoshi Kawata[†,‡]

[†]Nanophotonics Laboratory, RIKEN, 2-1 Hirosawa, Wako, Saitama 351-0198, Japan

[‡]Department of Applied Physics, Osaka University, 2-1 Yamadaoka, Suita, Osaka 565-0871, Japan

Supporting Information

ABSTRACT: The dielectric constant of indium in the deep-ultraviolet (DUV) region satisfies the conditions for localized surface plasmon resonance with low absorption loss. We report that indium acts as an agent of efficient surface-enhanced resonance Raman scattering (SERRS) in the DUV. Indium-coated SERRS substrates were prepared by depositing indium on fused silica glass substrates with control of the deposition thickness to tailor the plasmon resonance in the DUV. With excitation at 266 nm, SERRS was observed from thin adenine films deposited on the indium-coated substrates, and the signal intensity was up to 11 times higher than that of a bare fused silica glass substrate. FDTD calculations showed that an enhanced electromagnetic field can be locally generated on the indium-coated substrates. Considering the volume of the enhanced field region in the excitation spot, we estimated the average enhancement factor to be 10^2 or higher. Our results indicate that indium is a promising and easy-to-use metal for efficiently exciting DUV-SERRS of samples containing a small number of molecules.

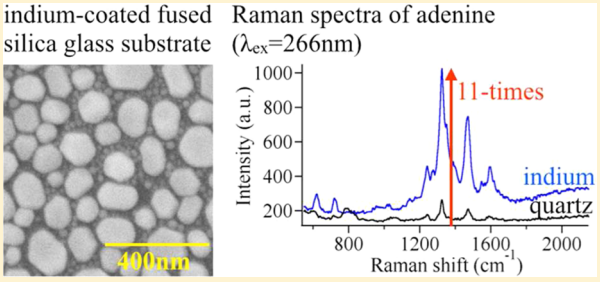

KEYWORDS: *indium, surface-enhanced resonance Raman scattering, localized surface plasmon resonances, deep-ultraviolet*

Surface-enhanced Raman scattering (SERS) is useful for label-free, nondestructive detection and analysis of samples containing a small number of molecules,[1−3] even single molecules.[4,5] Since its discovery in 1974,[6] SERS research has resulted in a large number of papers, exceeding 11 000,[7] mostly related to visible or near-infrared (NIR) light excitation. Recently, small but growing efforts have been made to extend SERS to the deep-ultraviolet (DUV) region. DUV excitation makes SERS more powerful for high S/N measurement of a small number of molecules. The advantages of DUV excitation are notable when measuring aromatic compounds such as nucleotide bases[8] and aromatic amino acid residues,[9] which are essential in biology. The scattering efficiency of these molecules is up to 10^6 times higher with DUV excitation compared with visible and NIR excitation[10] due to the resonance Raman effect. Additionally, DUV excitation can be used to distinguish Raman bands from native fluorescence of a sample in a spectrum.[11] Furthermore, since the light-scattering efficiency is inversely proportional to the fourth power of the wavelength, DUV excitation can give a 10−100 times stronger Raman scattering signal from any off-resonance molecule than visible and NIR excitation can.

Resonance excitation of localized surface plasmon polaritons (LSPPs) in metals is required for SERS.[12−15] Silver and gold, metals commonly used for SERS, cannot support the excitation of LSPPs in the DUV.[16] To extend SERS to the DUV, it is essential to explore DUV plasmonic metals, in which surface plasmons are resonantly excited by DUV light. So far, aluminum is recognized as the only reliable and efficient DUV plasmonic metal.[16−32] The usefulness of aluminum as a medium of LSPPs in the DUV was first demonstrated in 2007 via extraordinary optical transmission, a well-known plasmonic phenomenon.[17] The first demonstration of DUV (λ_{ex} = 244 nm) surface-enhanced resonance Raman scattering (SERRS) using aluminum was also reported in 2007.[18] In the following years, various nanostructures (sharp metallic tips,[16] nanodisks,[19] bowties,[20] and nanovoids[21]) of aluminum were developed and employed for practical applications of SERRS. The DUV plasmonic properties of aluminum have also been used for enhancement of fluorescence,[22,23] photoelectron emission,[24] and TiO_2 photocatalysis[25] with DUV excitation.

In spite of the recent increasing attention to SERS in the DUV, only aluminum thus far has been demonstrated as a reliable and efficient metal for SERS in the DUV. In this article we examine the potential of indium as a metal for SERS in the DUV and report that indium is a reliable and easy-to-use metal for greatly enhancing DUV resonance Raman scattering of analytes. Historically, indium was first examined as a metal to enhance luminescence[33] and Raman scattering[34−36] in the visible range in the 1980s; then it was predicted to enhance

Received: March 12, 2014
Published: June 10, 2014

Raman scattering in the DUV by electromagnetic simulations in 1987.[37] For more than 20 years after this prediction, indium has yet to be used for SERS in the DUV. Recently, a study of metal-enhanced fluorescence[38] and a numerical study of electromagnetic enhancement[39] by indium were reported, showing renewed consideration of indium as a plasmonic metal in the DUV. However, the potential of indium in the DUV has not been quantitatively and experimentally evaluated yet. A thorough study in the DUV is therefore necessary for indium, as used to be the case for aluminum, which was also predicted as a good metal for SERS in the UV in 1987[37] but has also been recently used in experiments[16−32] in the DUV.

Among many kinds of metals predicted to enhance Raman scattering in the DUV by Schatz,[37,39] we focused on indium because its dielectric function best satisfies two important criteria for high-gain and low-loss DUV plasmonic metals: (1) the real part of the dielectric function is smaller than −2[40] (see the inset of Figure 1) so that plasmons can resonantly couple

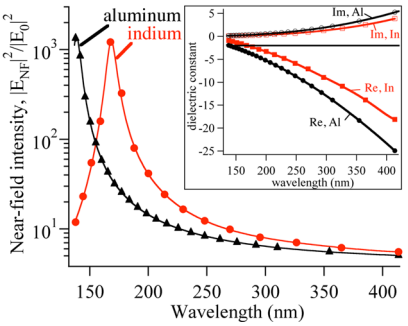

Figure 1. Near-field intensity induced by an external field (E_0) at the surface of indium spheres (red line and circles) and aluminum spheres (black line and triangles) whose diameters are much smaller than the wavelength of light. The near-field intensity is defined as $|E_{NF}|^2/|E_0|^2$, where $|E_{NF}|^2$ is the near-field intensity at the surface of the sphere, calculated with the quasi-electric approximation.[14] The inset shows the dielectric functions of indium[40] and aluminum.[41,42]

with DUV light in metallic nanostructures and (2) the imaginary part of the dielectric function[40] is smaller than that of aluminum;[41,42] that is, the absorption loss is smaller than that of aluminum. The low absorption loss in indium is ensured by the fact that the interband transition of indium (1.3 eV)[43] is as far from the DUV region as that of aluminum (1.5 eV).[44]

The potential of indium as an agent for efficient DUV-SERRS is shown by simple calculations of the near-field intensity induced by an external field at the surface of a sphere whose diameter is much smaller than the wavelength of light. The near-field intensity, $|E_{NF}|^2$, is calculated as a static field component of the dipole radiation emitted by the temporal oscillation of the polarizability derived from Mie theory under the quasi-electrostatic approximation.[14] The equation for the calculation is

$$|E_{NF}|^2 = |2(\varepsilon_1(\omega) - 1)/(\varepsilon_1(\omega) + 2)|^2 |E_0|^2$$

where $\varepsilon_1(\omega)$ is the dielectric function of the metal, and $|E_0|^2$ is the intensity of an external field. Solving the equation by substituting $\varepsilon_1(\omega)$ with the dielectric functions presented in the inset of Figure 1 yields the near-field intensity for indium and aluminum as a function of wavelength, as shown in Figure 1. According to the results, indium can support DUV-SERRS as efficiently as, or even more efficiently than, aluminum can. Besides the plasmonic property, there is another advantage of indium over aluminum as a SERRS agent. According to the literature,[38] indium forms multiple well-separated grains on a flat fused silica glass substrate via thermal vapor deposition in a vacuum without performing any treatment on the substrate. A substrate with well-separated grains has good surface roughness and a number of gaps where "hot spots" are produced and is, therefore, suitable for exciting reproducible and intense SERS.[45] On the other hand, aluminum tends to form a flat surface and requires treatment to form a rough surface, such as the use of a patterned substrate[32] and substrate annealing.[46]

Experimentally, we thermally evaporated and deposited indium (wire with purity of 99.99%, Nilaco, Inc.) on a fused silica glass substrate in a vacuum chamber (10^{-4} Pa). The thickness and rate of indium deposition were monitored with a quartz crystal unit. The deposition rate was set to 0.5 Å/s. After thermal deposition, the vacuum chamber was cooled to room temperature to avoid oxidation of the indium when exposed to the air. Indium can be coated with thick (>10 nm) oxidation layers in air at high temperature.[47] In the deposition process, we expected to be able to tailor the size of the indium grains by controlling the deposition thickness.[38] Figure 2a−h shows SEM images of the indium-coated substrates prepared with deposition thicknesses of 5, 10, 15, 20, 25, 30, 40, and 50 nm. Indium formed multiple grains under all conditions. As expected, the grain size depended on the deposition thickness. Interestingly, small grains appeared in the spaces among larger grains, except for the 5 and 10 nm indium-coated substrates. Formation of the small grains can be understood as a result of merging of indium grains formed on the glass at the beginning of the deposition process and revealing of glass for small grains to be formed as the deposition thickness increases.[38] The idea

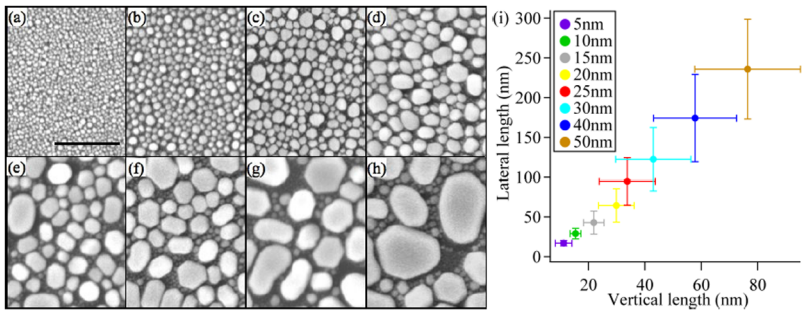

Figure 2. Indium-coated substrates prepared with thermal vapor deposition. (a−h) SEM images of multigrain indium-coated substrates prepared with deposition thicknesses of 5, 10, 15, 20, 25, 30, 40, and 50 nm, respectively. The scale bar is 0.4 μm. (i) Average vertical and lateral lengths of indium grains formed in each substrate. Error bars represent the standard deviations.

dx.doi.org/10.1021/ph500076k | ACS Photonics 2014, 1, 598−603

of this mechanism suggested that the size of the small grains in the 15, 20, 25, 30, 40, and 50 nm indium-coated substrates can be independent of the deposition thickness. We excluded small particles in those six substrates when analyzing the average size of the indium grains in each substrate. Thus, we statistically analyzed both the lateral and the vertical lengths of grains seen in SEM and AFM images (data not shown), respectively. Figure 2i represents the resultant averages of the lateral and vertical lengths of 30 grains for each substrate. Both the lateral and vertical lengths of indium grains (excluding the small grains existing in the spaces between the larger grains) monotonically increased as the deposition thickness of indium increased.

To examine the plasmonic properties of the indium-coated substrates, we measured their extinction spectra with a UV−vis spectrometer (UV-3600, Shimadzu, Inc.). Figure 3a presents

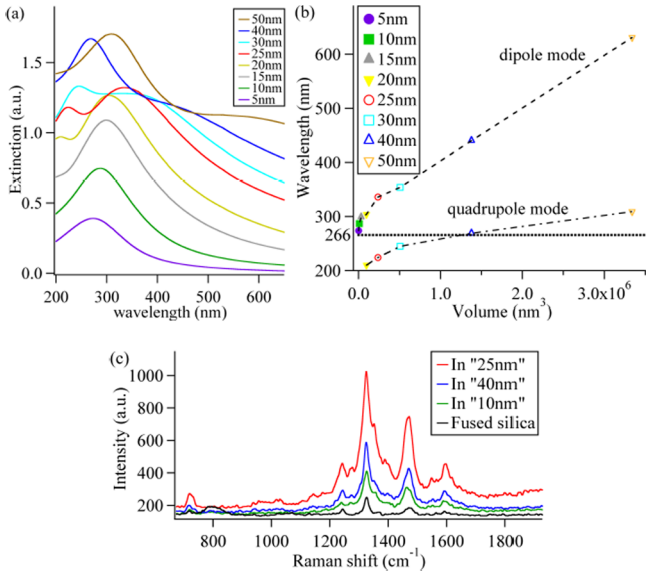

Figure 3. (a) Extinction spectra of the indium-coated substrates prepared with deposition thicknesses of 5, 10, 15, 20, 25, 30, 40, and 50 nm. (b) Extinction peak wavelength as a function of the average volume of the indium grains. The dashed line is at 266 nm, the laser line used for exciting SERRS. (c) Raman spectra of thin adenine films formed with equal thicknesses on the indium-coated substrates prepared with deposition thicknesses of 10, 25, and 40 nm and on a bare fused silica glass substrate.

extinction spectra of the indium-coated substrates prepared with deposition thicknesses of 5, 10, 15, 20, 25, 30, 40, and 50 nm. All the spectra have one or two extinction bands in the DUV. These bands are attributable to localized surface plasmon resonances of indium. The single peaks observed in the spectra for the 5, 10, and 15 nm indium-coated substrates and the longer wavelength peaks in the spectra for the other substrates are assigned to dipole modes, whereas the shorter wavelength peaks in the spectra for the 20, 25, 30, 40, and 50 nm indium-coated substrates are assigned to quadrupole modes. Figure 3b summarizes the peak wavelength of the extinction band as a function of the average volume of the indium grains. The average volume was estimated by assuming pillar-like grain structures with a diameter equal to the average lateral length and a height equal to the average vertical length, shown in Figure 2i. The upper and lower plots represent plasmon resonances of quadrupole and dipole modes, respectively. Both dipole and quadrupole peak wavelengths monotonically red-shifted with an increase in volume of the indium grains. Since we ignored the small grains, the results can mean that the extinction spectra are dominantly due to the large grains. Thus, the plasmon resonance wavelength of the indium-coated substrates can be tailored to the DUV by size control of the indium grains via control of the deposition thickness.

Using the prepared substrates, we examined the ability of indium to enhance resonance Raman scattering in the DUV. As a test sample, we selected adenine, because it efficiently scatters DUV light by the resonance Raman effect. Adenine is important in biology, as one of the nucleotide bases, and is a common sample used in research on DUV-SERRS[16,19,21] since it forms a thin film with a uniform thickness, which is useful for quantitative evaluation of the SERRS enhancement factor. Using a vapor deposition method,[19] we formed uniform, thin (1 nm) adenine films on indium-coated substrates prepared as described above, as well as on a bare fused silica glass substrate as a reference (see SI). In the Raman measurements, a diode-pumped solid-state laser with CW emission at a wavelength of 266 nm (MBD-266, Coherent, Inc.) was used as the excitation light source. This wavelength matched an absorption peak of adenine lying at ∼270 nm (see Figure S1). A laser beam with a power of 1 μW was focused onto the sample by a DUV microscope objective lens (40×, Thorlabs, Inc.) with an NA = 0.4. The scattered light from the sample was collected with a backscattering configuration. After Rayleigh rejection by an edge-filter, Raman scattered light was collected by a spectrometer (Acton SP2500, Princeton Instruments, Inc.) equipped with a grating having 1800 G/mm and was detected in the form of a spectrum with a back-illuminated, cooled DUV CCD camera (PyLoN:2KBUV, Princeton Instruments, Inc.). The grating dispersion was calibrated with the laser line (0 cm^{-1}) and the Raman bands of boron nitride (1364 cm^{-1}) and acetonitrile (2249 cm^{-1}). For each single spectral measurement, we accumulated signals from 100 different positions separated from neighboring positions by 10 μm on the substrate. Accumulation of signals from different positions is essential to gain a high S/N sufficient for quantitative analysis of the Raman band intensity without sample photodegradation.[19,48] Since the fwhm of the focus profile was 0.4 μm, we estimated the in-plane cross-sectional area of the focus spot to be 0.13 μm^2 and therefore, estimated the total observation area to be 13 μm^2.

Figure 3c shows measured Raman spectra of adenine films formed with equal thicknesses on the bare fused silica glass substrate and on the 10, 25, and 40 nm indium-coated substrates. According to Figure 3b, the 10 and 40 nm indium-coated substrates showed plasmon resonances due to a dipole mode and a quadrupole mode, respectively, in the wavelength range of the excitation and the scattering (266−280 nm), whereas for the 25 nm indium-coated substrate, the wavelength range was in the middle between the bands of the dipole and quadrupole modes. In the spectra, outstanding peaks were observed at 720, 1250, 1330, 1470, and 1600 cm^{-1}, all attributable to Raman scattering of adenine vibrations. All three indium-coated substrates showed higher intensities of these bands compared with those of the fused silica substrate. The largest enhancement was observed with the 25 nm indium-coated substrate. For quantitative evaluation of the enhancement, the intense and well-isolated band at 1469 cm^{-1}, attributable to the combination tone of C4N9 stretching and C8H bending vibrations,[10] was analyzed. The band was fitted to a Lorentz function, and the area of the band was derived. The

dx.doi.org/10.1021/ph500076k | ACS Photonics 2014, 1, 598−603

band area was compared between the indium-coated and fused silica substrates to examine the Raman enhancement, defined as the ratio of the band area for an indium-coated substrate to that for the fused silica glass substrate (I_{In}/I_{FS}). In comparison, we found the largest enhancement to be 11 times for the 25 nm indium-coated substrate. The enhancement for the 10 and 40 nm indium-coated substrates was 1.9 and 5.2 times, respectively.

According to experiments, the largest enhancement was not observed with the 10 or 40 nm indium-coated substrate, in which the plasmon resonances lie exactly in the excitation and scattering wavelength ranges. Reports in the literature showed that the SERS excitation profile and the extinction spectrum of a SERS substrate do not match in a complex system, such as a grainy metal substrate.[49,50] This is because the SERS spectrum will be dominated by the resonances involving "hot spots", whereas the extinction spectrum of the SERS substrate will include contributions from the entire nanostructure.[7] This explanation is reasonable, and therefore, below we discuss the effects such hot spots, which can exist over the indium-coated substrates, on Raman enhancement.

The hot spots can be generated by coupling of larger and smaller grains, since a larger grain can serve as an antenna and a smaller grain can generate a strong near-field.[50,51] In this point, the 25 and 40 nm indium substrates are suitable for large enhancement of Raman scattering since they have many smaller grains in the spaces among larger grains, whereas the 10 nm indium-coated substrates are not. The hot spots can also be generated by gaps that are relatively small compared with the grain size. To discuss the effects of gaps on Raman enhancement for each substrate, we summarized, in Table 1,

Table 1. Average Information on Geometry and Alignment of 30 Grains for the 10, 25, and 40 nm Indium-Coated Substrates

deposition thickness (nm)	W (nm)	G_{all} (nm)	G_{cl} (nm)	G_{all}/W	G_{cl}/W	N_{gr}	N_{gap}
10	29	19	5.8	0.66	0.20	63	217
25	95	36	6.0	0.38	0.063	8.5	36
40	174	86	13	0.49	0.075	3.1	15

average information on the geometry and alignment of 30 grains, excluding small ones, for the 10, 25, and 40 nm indium-coated substrates taken from an SEM image of each substrate. W is the lateral length of the grains, taken from Figure 2i, G_{cl} and G_{all} are the size of the gap to the closest grain and the average size of the gaps to all neighboring grains, respectively, G_{cl}/W and G_{all}/W are gap sizes normalized to the lateral length of the grains, N_{gr} is the number of grains in the excitation spot, derived as the product of the cross-sectional area of the excitation spot and the density of the indium grains on the substrate, and N_{gap} is the number of gaps in the excitation spot, estimated from the density of grains and the number of neighboring grains for each grain. Both G_{all}/W and G_{cl}/W were the smallest for the 25 nm indium-coated substrate, whereas they were the largest for the 10 nm indium-coated substrate, meaning that the field will be locally enhanced at gaps on the 25 nm indium-coated substrate but not on the 10 nm indium-coated substrate. Comparing the 25 and 40 nm indium-coated substrates, the difference in N_{gap} in the excitation spot is prominent; the 25 nm indium-coated substrate had a larger number of gaps in the excitation spot than the 40 nm indium-coated substrate did. To summarize, the 25 nm indium-coated substrate was the best substrate for producing a larger number of strong hot spots.

FDTD calculations support the finding that an intense electromagnetic field can be generated on the 25 nm indium-coated substrate. We calculated the electromagnetic field distribution on a multigrain indium-coated substrate based on an SEM image of an indium-coated substrate prepared with a deposition thickness of 25 nm (see SI). The original SEM image and the model of the multigrain indium-coated substrate are shown in Figure 4a and b, respectively. Some of the small

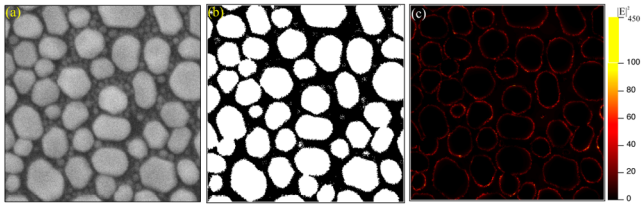

Figure 4. (a) SEM image of a 25 nm indium-coated substrate used to simulate (b) an indium-coated multigrain substrate for FDTD calculations. Here (b) is derived from (a) by image processing for intensity thresholding. (c) Calculated field intensity distribution at λ = 266 nm in a thin adenine film formed on the substrate in (b).

grains and the small gaps are not reproduced in the model. This is because the SEM image was processed with intensity thresholding so that each grain was separated. Through this process, the grain size was reduced and the gap size was enlarged compared with the experiments. We assumed each grain is a pillar with a height of 34 nm, which is the average height shown in Figure 2i for the 25 nm indium-coated substrate. Considering that adenine can exist only on top of indium grains and on the fused silica glass, but not inside the grains or in the air, we first calculated the field intensity distribution at λ = 266 nm at the plane defined by the top surface of the grains and the plane defined by the indium/glass boundary (see SI), and then we merged them to derive one image showing the field distribution in the adenine thin film. The resultant image is shown in Figure 4c. The figure indicates that the electromagnetic field is enhanced by the order of magnitude of 2. Since the modeled indium-coated substrate omits most of the small particles and gaps, which can generate local enhanced fields, the local enhancement factor in the experiments can be higher than this calculated value.

The calculated field distribution is also useful for estimating the average enhancement factor (η) in the experiment. The average enhancement factor is calculated through the following equation:

$$\eta = (I_{In}/I_{FS} + V_{SERRS} - 1)/V_{SERRS}$$

where V_{SERRS} is the relative volume of hot spots in the excitation spot to the total volume of the excitation spot, and I_{In}/I_{FS} is 11 for the 25 nm indium-coated substrate. V_{SERRS} can be estimated from the area occupied by hot spots relative to the total area in the calculated field distribution. According to Figure 4c, the strongly enhanced field can be localized in the circumference of the indium grains. The area of the strongly enhanced field region is estimated to be ~10% of the in-plane cross-sectional area of the focus spot. Assuming that most of the SERRS signal could arise from this region, V_{SERRS} could be determined to be 0.1. Thus, we estimated η to be 10^2. This is a

dx.doi.org/10.1021/ph500076k | ACS Photonics 2014, 1, 598−603

similar order of magnitude to the value for aluminum,[19] even though tight localization of the enhanced field is not considered in this estimation.

In summary, we discovered that indium acts as an agent for enhancing DUV-SERRS of organic molecules. Indium-coated SERRS substrates were prepared by depositing indium on fused silica glass substrates only with control of the deposition thickness to tailor the plasmon resonance in the DUV. With excitation at a wavelength of 266 nm, SERRS was observed from thin adenine films deposited on the indium-coated substrates. The Raman scattering signal of the adenine deposited on the indium-coated substrates was up to 11 times higher than that of a bare fused silica glass substrate. FDTD calculations indicated that the enhanced electromagnetic field can be locally distributed in a limited region on the substrates. According to the calculated field distribution, we estimated the average enhancement factor to be 10^2 or higher. The enhancement factor in the experiment can be much higher because the calculations omitted small gaps and grains where a strongly enhanced field can be tightly localized. Our results show that indium is an efficient and easy-to-use metal for exciting DUV-SERRS and will accelerate the development of research applications in DUV-SERRS by extending the choice of metal that can be used.

■ ASSOCIATED CONTENT

Supporting Information

Details of formation of adenine thin films, evaluation of thickness of adenine films, and simulations of field distribution of an indium-coated substrate. This material is available free of charge via the Internet at http://pubs.acs.org.

■ AUTHOR INFORMATION

Corresponding Author

*E-mail: yuika@ap.eng.osaka-u.ac.jp.

Notes

The authors declare no competing financial interest.

■ ACKNOWLEDGMENTS

This work was financially supported by JSPS Grant-in-Aid for Scientific Research (S) 21226003.

■ REFERENCES

(1) Campion, A.; Kambhampati, P. Surface-enhanced Raman scattering. *Chem. Soc. Rev.* **1998**, *27*, 241−250.
(2) Kneipp, K.; Kneipp, H.; Itzkan, I.; Dasari, R. R.; Feld, M. S. Ultrasensitive chemical analysis by Raman spectroscopy. *Chem. Rev.* **1999**, *99*, 2957−2975.
(3) Moskovits, M. Surface-enhanced Raman spectroscopy: a brief perspective. In *Surface-Enhanced Raman Scattering - Physics and Applications*; Kneipp, K.; Moskovits, M.; Kneipp, H., Eds.; Topics in Applied Physics Vol. 103; Springer-Verlag: Berlin, 2006; pp 1−17.
(4) Nie, S.; Emory, S. R. Probing single molecules and single nanoparticles by surface-enhanced Raman scattering. *Science* **1997**, *275*, 1102−1106.
(5) Kneipp, K.; Wang, Y.; Kneipp, H.; Perelman, L. T.; Itzkan, I.; Dasari, R. R.; Feld, M. S. Single molecule detection using surface-enhanced Raman scattering (SERS). *Phys. Rev. Lett.* **1997**, *78*, 1667−1670.
(6) Fleischmann, M.; Hendra, P. J.; McQuillan, A. J. Raman spectra of pyridine adsorbed at a silver electrode. *Chem. Phys. Lett.* **1974**, *26*, 163−166.
(7) Moskovits, M. Persistent misconceptions regarding SERS. *Phys. Chem. Chem. Phys.* **2013**, *15*, 5301−5311.
(8) Fodor, S. R. A.; Rava, R. P.; Hays, T. R.; Spiro, T. G. Ultraviolet resonance Raman spectroscopy of the nucleotides with 266-, 240-, 218-, and 200-nm pulsed laser excitation. *J. Am. Chem. Soc.* **1985**, *107*, 1520−1529.
(9) Johnson, C. R.; Ludwig, M.; O'Donnell, S.; Asher, S. A. UV resonance Raman spectroscopy of the aromatic amino acids and myoglobin. *J. Am. Chem. Soc.* **1984**, *106*, 5008−5010.
(10) Wen, Z. Q.; Thomas, G. J., Jr. UV resonance Raman spectroscopy of DNA and protein constituents of viruses: assignments and cross sections for excitations at 257, 244, 238, and 229 nm. *Biopolymers* **1998**, *45*, 247−256.
(11) Asher, S. A.; Johnson, C. R.; Murtaugh, J. Development of a new UV resonance Raman spectrometer for the 217−400-nm spectra region. *Rev. Sci. Instrum.* **1983**, *54*, 1657−1662.
(12) Moskovits, M. Surface roughness and the enhanced intensity of Raman scattering by molecules adsorbed on metals. *J. Chem. Phys.* **1978**, *69*, 4159−4161.
(13) Jeanmaire, D. L.; Van Duyne, R. P. Surface Raman spectroelectrochemistry part I. Heterocyclic aromatic, and aliphatic amines adsorbed on the anodized silver electrode. *J. Electroanal. Chem.* **1977**, *84*, 1−20.
(14) Schatz, G. C.; Van Duyne, R. P. Electromagnetic mechanisms of surface-enhanced spectroscopy. In *Handbook of Vibrational Spectroscopy*; Chalmers, J. M.; Griffiths, P. R., Eds.; Wiley: New York, 2002; pp 759−774.
(15) Albrecht, M. G.; Creighton, J. A. Anomalously intense Raman spectra of pyridine at a silver electrode. *J. Am. Chem. Soc.* **1977**, *99*, 5215−5217.
(16) Taguchi, A.; Hayazawa, N.; Furusawa, K.; Ishitobi, H.; Kawata, S. Deep-UV tip-enhanced Raman scattering. *J. Raman Spectrosc.* **2009**, *40*, 1324−1330.
(17) Ekinci, Y.; Solak, H. H.; David, C. Extraordinary optical transmission in the ultraviolet region through aluminum hole arrays. *Opt. Lett.* **2007**, *32*, 172−174.
(18) Doerfer, T.; Schmitt, M.; Popp, J. Deep-UV surface-enhanced Raman scattering. *J. Raman Spectrosc.* **2007**, *38*, 1379−1382.
(19) Jha, S. K.; Ahmed, Z.; Agio, M.; Ekinci, Y.; Loeffler, J. F. Deep-UV surface-enhanced resonance Raman scattering of adenine on aluminum nanoparticle arrays. *J. Am. Chem. Soc.* **2012**, *134*, 1966−1969.
(20) Li, L.; Lim, S. F.; Puretzky, A. A.; Riehn, R.; Hallen, H. D. Near-field enhanced ultraviolet resonance Raman spectroscopy using aluminum bow-tie nano-antenna. *Appl. Phys. Lett.* **2012**, *101*, 113116.
(21) Sigle, D. O.; Perkins, E.; Baumberg, J. J.; Mahajan, S. J. Reproducible deep-UV SERRS on aluminum nanovoids. *Phys. Chem. Lett.* **2013**, *4*, 1449−1452.
(22) Ray, K.; Chowdhury, M. H.; Lakowicz, J. R. Aluminum nanostructured films as substrates for enhanced fluorescence in the ultraviolet-blue spectral region. *Anal. Chem.* **2007**, *79*, 6480−6487.
(23) Ono, A.; Kikawada, M.; Akimoto, R.; Inami, W.; Kawata, Y. Fluorescence enhancement with deep-ultraviolet surface plasmon excitation. *Opt. Express* **2013**, *21*, 17447−17453.
(24) Watanabe, Y.; Inami, W.; Kawata, Y. Deep-ultraviolet light excites surface plasmon for the enhancement of photoelectron emission. *J. Appl. Phys.* **2011**, *109*, 023112.
(25) Honda, M.; Kumamoto, Y.; Taguchi, A.; Saito, Y.; Kawata, S. Plasmon-enhanced UV photocatalysis. *Appl. Phys. Lett.* **2014**, *104*, 061108.
(26) Knight, M. W.; King, N. S.; Liu, L.; Everitt, H. O.; Nordlander, P.; Halas, N. J. Aluminum for plasmonics. *ACS Nano* **2014**, *8*, 834−840.
(27) Langhammer, C.; Schwind, M.; Kasemo, B.; Zoric, I. Localized surface plasmon resonances in aluminum nanodisks. *Nano Lett.* **2008**, *8*, 1461−1471.
(28) Chan, G. H.; Zhao, J.; Schatz, G. C.; Van Duyne, R. P. Localized surface plasmon resonance spectroscopy of triangular aluminum nanoparticles. *J. Phys. Chem. C* **2008**, *112*, 13958−13963.

(29) Ekinci, Y.; Solak, H. H.; Loeffler, J. F. Plasmon resonances of aluminum nanoparticles and nanorods. *J. Appl. Phys.* **2008**, *104*, 083107.
(30) Taguchi, A.; Saito, Y.; Watanabe, K.; Yijian, S.; Kawata, S. Tailoring plasmon resonances in the deep-ultraviolet by size-tunable fabrication of aluminum nanostructures. *Appl. Phys. Lett.* **2012**, *101*, 081110.
(31) Knight, M. W.; Liu, L.; Wang, Y.; Brown, L.; Mukherjee, S.; King, N. S.; Everitt, H. O.; Nordlander, P.; Halas, N. J. Aluminum plasmonic nanoantennas. *Nano Lett.* **2012**, *12*, 6000−6004.
(32) Maidecchi, G.; Conella, G.; Zaccaria, R. P.; Moroni, R.; Anghiolfi, L.; Giglia, A.; Nanarone, S.; Mattera, L.; Dai, H.-L.; Canepa, M.; Bisio, F. Deep-ultraviolet plasmon resonance in aluminum nanoparticle arrays. *ACS Nano* **2013**, *7*, 5834−5841.
(33) Loufty, R. O.; Aroca, R. Interaction of indium metal with phthalocyanine molecules: luminescence enhancement. *J. Luminesc.* **1982**, *26*, 359−366.
(34) Jennings, C.; Aroca, R.; Hor, A.-M.; Loutfy, R. O. Surface-enhanced Raman scattering from copper and zinc phthalocyanine complexes by silver and indium island films. *Anal. Chem.* **1984**, *56*, 2033−2035.
(35) Aroca, R.; Jennings, C.; Kovacs, G. J.; Loutfy, R. O.; Vincett, P. S. Surface-enhanced Raman scattering of Langmuir-Blodgett monolayers of phthalocyanine by indium and silver island films. *J. Phys. Chem.* **1985**, *89*, 4051−4054.62.
(36) Moskovitz, M. Surface-enhanced spectroscopy. *Rev. Mod. Phys.* **1985**, *57*, 783−826.
(37) Zeman, E. J.; Schatz, G. C. An accurate electromagnetic theory study of surface enhancement factors of Ag, Au, Cu, Li, Na, Al, Ga, In, Zn, and Cd. *J. Phys. Chem.* **1987**, *91*, 634−643.
(38) Dragan, A. I.; Geddes, C. D. Indium nanodeposits: A substrate for metal-enhanced fluorescence in the ultraviolet spectral region. *J. Appl. Phys.* **2010**, *108*, 094701.
(39) McMahon, J. M.; Schatz, G. C.; Gray, S. K. Plasmonics in the ultraviolet with the poor metals Al, Ga, In, Sn, Tl, Pb, and Bi. *Phys. Chem. Chem. Phys.* **2013**, *15*, 5415−5423.
(40) Lemonnier, J. C.; Jezequel, G.; Thomas, J. Optical properties in the far UV and electronic structure of indium films. *J. Phys. C: Solid State Phys.* **1975**, *8*, 2812−2818.
(41) Shiles, E.; Sasaki, T.; Inotuki, M.; Smith, D. Y. Self-consistency and sum-rule tests in the Kramers-Kronig analysis of optical data: Applications to aluminum. *Phys. Rev. B* **1980**, *22*, 1612−1628.
(42) Smith, D. Y.; Shiles, E.; Inokuti, M. The optical properties of metallic aluminum. In *Handbook of Optical Constants of Solids: Vol. 1*; Palik, E. D., Ed.; Academic Press Handbook Series; Academic Press: Orlando, FL, 1985; pp 369−406.
(43) Theye, M. L.; Devant, G. The optical properties of indium from thin film measurements. *Thin Solid Films* **1969**, *4*, 205−210.
(44) Ehrenreich, H.; Philipp, H. R.; Segall, B. Optical properties of aluminum. *Phys. Rev.* **1963**, *132*, 1918−1928.
(45) Wang, H.-H.; Liu, C.-Y.; Wu, S.-B.; Liu, N.-W.; Peng, C.-Y.; Chan, T.-H.; Wang, J.-K.; Wang, Y.-L. Highly Raman-enhancing substrates based on silver nanoparticle arrays with tunable sub-10 nm gaps. *Adv. Mater.* **2006**, *18*, 491−495.
(46) Villesen, T. F.; Uhrenfeldt, C.; Johansen, B.; Nylandsted Larsen, A. Self-assembled Al nanoparticles on Si and fused silica, and their application for Si solar cells. *Nanotechnology* **2013**, *24*, 275606.
(47) Schoeller, H.; Cho, J. Oxidation and reduction behavior of pure indium. *Mater. Res.* **2009**, *24*, 386−393.
(48) Kumamoto, Y.; Taguchi, A.; Smith, N. I.; Kawata, S. Deep UV resonant Raman spectroscopy for photodamage characterization in cells. *Biomed. Opt. Express* **2011**, *2*, 927−936.
(49) Doherty, M. D.; Murphy, A.; McPhillips, J.; Pollard, R. J.; Dawson, P. Wavelength dependence of Raman enhancement from gold nanorod arrays: quantitative experiment and modeling of a hot spot dominated system. *J. Phys. Chem. C* **2010**, *114*, 19913−19919.
(50) Yang, Y.; Callahan, J. M.; Kim, T.-H.; Brown, A. S.; Everitt, H. O. Ultraviolet nanoplasmonics: a demonstration of surface-enhanced Raman spectroscopy, fluorescence, and photodegradation using gallium nanoparticles. *Nano Lett.* **2013**, *13*, 2837−2841.
(51) Sun, G.; Khurgin, J. B. Optimization of the nanolens consisting of coupled metal nanoparticles: an analytical approach. *Appl. Phys. Lett.* **2011**, *98*, 153115.